JOURNAL OF THERMOPHYSICS AND HEAT TRANSFER
Vol. 16, No. 4, October–December 2002

Thermocapillary Convection in Liquid Bridges with Undeformable Curved Surfaces

Bok-Cheol Sim* and Abdelfattah Zebib†
Rutgers University, Piscataway, New Jersey 08854-8058

Thermocapillary convection in differentially heated cylindrical liquid bridges is investigated by two- and three-dimensional numerical simulations. The nondeformable free surface is either flat or curved as determined by the fluid volume and the Young–Laplace equation. With Prandtl numbers of 1 and 4 and a flat surface, our computed results for onset of oscillations are in good agreement with linear theory. Convection is steady and axisymmetric at sufficiently low values of Reynolds number with either flat or curved interfaces. Only steady convection is possible at all Reynolds numbers considered in strictly axisymmetric computations. Transition to oscillatory three-dimensional motions occurs as the Reynolds number increases beyond a critical value, dependent on the Prandtl number and liquid volume. Rotating waves with wave numbers of 1 or 2 are observed. The critical wave number depends on the Biot number. Heat loss from the free surface stabilizes the flow, and the critical Reynolds number increases with increasing Biot number. With nonzero Biot number, two different branches can exist in the stability diagram. The numerical results are in reasonable agreement with experiments.

Nomenclature

AR	=	aspect ratio, R/H
Bi	=	Biot number, hH/k
Ca	=	capillary number, $\gamma\Delta T/\sigma_0$
F	=	nondimensional frequency
f	=	dimensional frequency, Hz
H	=	height of the liquid bridge
h	=	heat transfer coefficient
k	=	thermal conductivity
Ma	=	Marangoni number, $Pr \cdot Re$
m	=	wave number
P	=	nondimensional pressure
Pr	=	Prandtl number, ν/α
R	=	radius of the liquid bridge
Re	=	Reynolds number, $\gamma\Delta TH/\nu\mu$
Re_c	=	critical Reynolds number
R_r	=	nondimensional neck radius, (minimum radius)$/H$
r	=	radial direction
T	=	nondimensional temperature
u	=	nondimensional radial velocity
V	=	nondimensional liquid volume
v	=	nondimensional axial velocity
$\boldsymbol{v}$	=	nondimensional velocity vector
w	=	nondimensional azimuthal velocity
z	=	axial or vertical direction
α	=	thermal diffusivity
γ	=	$-\partial\sigma/\partial T$
ΔT	=	characteristic T, $T_h - T_c$
θ	=	azimuthal direction
μ	=	dynamic viscosity
ν	=	kinematic viscosity
ρ	=	density
σ	=	surface tension
ω_c	=	nondimensional critical angular frequency, $2\pi f H^2/\nu$

Introduction

THERMOCAPILLARY convection is a surface-tension-driven flow created by a temperature gradient along a free surface. It is well known that thermocapillary convection is steady (and axisymmetric) when the temperature difference between two side walls of an open cavity (or two disks of a liquid bridge) is sufficiently small. This steady flow undergoes a transition to oscillatory time-dependent, three-dimensional convection as the temperature difference increases beyond a critical value. To obtain homogeneous solids from crystal melt, the influence of buoyancy and thermocapillary forces needs to be understood. These forces cause convection in the melt during crystal growth on Earth. However, in a microgravity environment, thermocapillary forces dominate and may drive unsteady convection that is responsible for striations in the crystal. Therefore, understanding transition to oscillatory flows is important to material processing in space. Marangoni effects in the floating zone, Czochralski technique, and open boat zone were summarized by Schwabe.[1]

There have been a large number of experimental studies on surface-tension-driven convection in liquid bridges. Preisser et al.[2] proved experimentally the occurrence of oscillatory convection in a liquid bridge with $Pr = 8.9$. They observed waves traveling in the azimuthal direction and a unique wave number of about 2 regardless of aspect ratio. Velten et al.[3] found that buoyant forces could stabilize thermocapillary convection in a liquid bridge by comparing results heated from above with those from below and observed the effect of aspect ratio on the critical Reynolds number and frequency. Carotenuto et al.[4] reported on standing waves with a wave number m of 1 in microgravity experiments. Secondary instabilities to rotating from pulsating waves and to $m = 2$ from $m = 1$ were experimentally reported by Monti et al.[5] and Muehlner et al.,[6] respectively. Transition to a chaotic thermocapillary flow was observed by Schwabe and Frank.[7] Schwabe and Velten[8] reported restationarization above a critical Marangoni number in a long floating zone.

The influence of the free surface shape as determined by the liquid volume was experimentally studied by Hu et al.,[9] Masud et al.,[10] Shevtsova et al.,[11] and Sumner et al.[12] It is evident from the experiments that two branches exist in a stability diagram (ΔT_c–V). The critical wave number could be switched from 1 to 2 by changing the surrounding conditions and, thus, the heat loss from the liquid bridge.[11]

Received 20 November 2001; revision received 19 April 2002; accepted for publication 19 April 2002.

*Teaching Assistant, Department of Mechanical and Aerospace Engineering; currently Postdoctoral Associate, Department of Mechanical Engineering, Hanyang University, Ansan-si 425-791, Republic of Korea.

†Professor, Department of Mechanical and Aerospace Engineering.

Smith and Davis[13] discussed the instability mechanisms by linear stability theory of flows in an infinite liquid layer. Linear stability in an infinite liquid bridge was investigated by Xu and Davis.[14] Kuhlmann and Rath[15] considered linear instability of steady axisymmetric thermocapillary flow in a liquid bridge with an aspect ratio of 1. They found that the most dangerous disturbance was either a pure hydrodynamic steady mode or an oscillatory hydrothermal wave, depending on Prandtl number Pr. Levenstam and Amberg[16] confirmed a first bifurcation from a steady axisymmetric flow to a steady nonaxisymmetric three-dimensional flow at low Prandtl number. Wanschura et al.[17] further investigated the primary instability of axisymmetric steady thermocapillary flow in a liquid bridge. They confirmed the earlier results of Neitzel et al.,[18] and provided a stability diagram for $Pr \leq 4.8$ with an aspect ratio of 1. Recently, a linear stability diagram for $Pr \leq 7$ was reported in detail by Levenstam et al.[19] Both diagrams are roughly in good agreement. The effect of liquid volume on instability in a liquid bridge was investigated by Chen and Hu.[20] However, their results of linear stability with a cylindrical surface and $Pr = 1$ were very different from those of other studies.[17–19]

Tao et al.[21] studied steady thermocapillary convection in a liquid bridge with a nondeformable curved surface by axisymmetric numerical simulations. Experimental and numerical studies on oscillatory convection with a cylindrical surface were reported by Savino and Monti.[22] They observed pulsating and rotating waves with a wave number of 1. Shevtsova and Legros[23] investigated oscillatory convection in deformed liquid bridges with $Pr = 105$ by axisymmetric numerical simulations. Whereas oscillatory buoyant-thermocapillary convection in the liquid bridge was reported with axisymmetric models, oscillatory thermocapillary convection with $Pr = 105$ was not found in the simulations.[23] Leypoldt et al.[24] showed that standing waves evolved into traveling waves with $Pr = 4$ and 7 by three-dimensional numerical simulations. The influence of temperature-dependent viscosity was reported by Shevtsova et al.[25] With $Pr = 35$, the effect of the temperature-dependent viscosity on the critical Reynolds number was less than 5% in their three-dimensional simulations.

Three-dimensional numerical simulations with undeformable curved surfaces have first been performed in a low Prandtl number liquid bridge by Lappa et al.[26] They studied the transition to steady nonaxisymmetric from axisymmetric flow with $Pr = 0.01$. Oscillatory thermocapillary convection with nondeformable curved surfaces were performed in an open cylinder by Sim and Zebib.[27] With $Pr = 30$, $AR = 1$, and $Bi = 0$, they showed that only steady thermocapillary convection with either flat or curved surfaces was possible in strictly axisymmetric computations, and the critical Reynolds number decreased with increasing liquid volume in the case of concave surfaces.

Although few experiments investigated the effect of the interface shape on time-dependent thermocapillary convection in a liquid bridge, this has not been reported in numerical studies. In the present paper, we report on thermocapillary convection in liquid bridges by two- and three-dimensional numerical simulations. The undeformable free surface is either flat or curved. The influence of the free surface shape and Prandtl number on the critical Reynolds number and frequency and the pattern of convection are investigated. The numerical results are then compared with those from linear theory and available experiments.

Mathematical Model

The physical system considered is a cylindrical liquid bridge with either flat or curved surface as shown in Fig. 1: $AR = 1$ and $Pr = 1$ and 4 are used to validate the numerical predictions with linear theory and $AR = 0.714$ and $Pr = 27$ to compare with experiments.[10] The upper and lower disks have dimensionless temperatures $T_h = 1$ and $T_c = 0$, respectively. The surface tension is assumed a linear function of temperature,

$$\sigma = \sigma_0 - \gamma(T - T_0) \tag{1}$$

where subscript 0 represents a reference state.

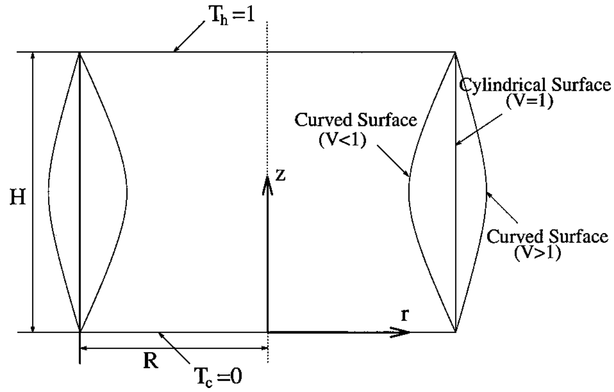

Fig. 1 Physical system.

In a microgravity environment, the nondimensional governing equations are as follows:

$$\nabla \cdot \boldsymbol{v} = 0 \tag{2}$$

$$Re\left[\frac{\partial \boldsymbol{v}}{\partial t} + \nabla \cdot (\boldsymbol{v}\boldsymbol{v})\right] = -\nabla P + \nabla^2 \boldsymbol{v} \tag{3}$$

$$Ma\left[\frac{\partial T}{\partial t} + \nabla \cdot (\boldsymbol{v}T)\right] = \nabla^2 T \tag{4}$$

Length, temperature, velocity, pressure, and time are normalized with respect to H, ΔT, $\gamma \Delta T/\mu$, $\gamma \Delta T/H$, and $\mu H/\gamma \Delta T$, respectively. The boundary conditions become, at $z = 0$,

$$u = 0, \qquad v = 0, \qquad w = 0, \qquad T = 0 \tag{5}$$

and, at $z = 1$,

$$u = 0, \qquad v = 0, \qquad w = 0, \qquad T = 1 \tag{6}$$

The nondimensionalized position of the free surface is described by a function $r = g(z)$. Thermal, kinematic, and tangential stress balance boundary conditions at the interface are

$$-\frac{1}{N}\left(\frac{\partial T}{\partial r} - g'\frac{\partial T}{\partial z}\right) = BiT \tag{7}$$

$$u = g'v \tag{8}$$

$$(1 - g'^2)\left(\frac{\partial v}{\partial r} + \frac{\partial u}{\partial z}\right) + 2g'\left(\frac{\partial u}{\partial r} - \frac{\partial v}{\partial z}\right) = -SN\left(g'\frac{\partial T}{\partial r} + \frac{\partial T}{\partial z}\right) \tag{9}$$

$$\frac{\partial w}{\partial r} - \frac{w}{r} + \frac{1}{r}\frac{\partial u}{\partial \theta} - g'\left(\frac{\partial w}{\partial z} + \frac{1}{r}\frac{\partial v}{\partial \theta}\right) = \frac{-SN}{r}\frac{\partial T}{\partial \theta} \tag{10}$$

where $N = (1 + g'^2)^{1/2}$ and $g' = dg/dz$. It is known that isotherms near hot and cold walls are compressed in high Prandtl number flow (see Ref. 28) and the driving force near the cold wall is much less effective for the overall flow than that near the hot wall.[10] The peak of the surface velocity near the cold wall generates difficulty for convergence in numerical simulations. Thus, in some of our numerical experiments, we use regularization (damping) near the cold wall only by changing the driving thermocapillary forces in Eqs. (9) and (10). The regularization factor[23] S in the lower 5% of the free surface at $z \leq 0.05$ is defined as

$$S = 0.25[1 - \cos(20\pi z)]^2 \tag{11}$$

and otherwise

$$S = 1 \tag{12}$$

The effect of this regularization on critical Reynolds number and frequency will be discussed.

The location of the interface $g(z)$ is determined by the normal stress balance. The deviation of the free surface shape from the static meniscus is characterized by Ca. When $Ca \ll 1$, the dynamic surface deformation can be neglected,[29] and the normal stress balance equation simplifies to the Young–Laplace equation. The interface and liquid volume equations in a state of rest are as follows:

$$-Ca\Delta P = \frac{1}{N}\left(\frac{g''}{N^2} - \frac{1}{g}\right) \tag{13}$$

$$V = \frac{1}{\mathit{AR}^2}\int_0^1 g^2\,\mathrm{d}z \tag{14}$$

where $\Delta P = P - P_0$ is the nondimensional pressure difference between the interface liquid and gas pressures, and the liquid volume is normalized with respect to $\pi R^2 H$. Equation (13) has two boundary conditions, $g(0) = \mathit{AR}$ and $g(1) = \mathit{AR}$. The shape of the interface and ΔP are fixed with a prescribed liquid volume.

Numerical Aspects

To solve the problem with a curved surface, the governing equations are transformed from the physical domain (r, z, θ) into a rectangular computational domain (ξ, η, ζ):

$$\xi = r/g(z) \tag{15}$$

$$\eta = z \tag{16}$$

$$\zeta = \theta \tag{17}$$

The governing equations transformed into the computational domain are

$$\frac{1}{\xi}\frac{\partial \xi u}{\partial \xi} - \xi g'\frac{\partial v}{\partial \xi} + g\frac{\partial v}{\partial \eta} + \frac{1}{\xi}\frac{\partial w}{\partial \zeta} = 0 \tag{18}$$

$$Re\left[\frac{\partial u}{\partial t} + \frac{1}{\xi g}\frac{\partial \xi u^2}{\partial \xi} - \frac{\xi g'}{g}\frac{\partial uv}{\partial \xi} + \frac{\partial uv}{\partial \eta} + \frac{1}{\xi g}\frac{\partial uw}{\partial \zeta} - \frac{w^2}{\xi g}\right]$$
$$= -\frac{1}{g}\frac{\partial p}{\partial \xi} - \frac{u}{(g\xi)^2} + \nabla^2 u - \frac{2}{(g\xi)^2}\frac{\partial w}{\partial \zeta} \tag{19}$$

$$Re\left[\frac{\partial v}{\partial t} + \frac{1}{\xi g}\frac{\partial \xi uv}{\partial \xi} - \frac{\xi g'}{g}\frac{\partial v^2}{\partial \xi} + \frac{\partial v^2}{\partial \eta} + \frac{1}{\xi g}\frac{\partial vw}{\partial \zeta}\right]$$
$$= -\frac{\partial p}{\partial \eta} + \frac{\xi g'}{g}\frac{\partial p}{\partial \xi} + \nabla^2 v \tag{20}$$

$$Re\left[\frac{\partial w}{\partial t} + \frac{1}{\xi g}\frac{\partial \xi uw}{\partial \xi} - \frac{\xi g'}{g}\frac{\partial vw}{\partial \xi} + \frac{\partial vw}{\partial \eta} + \frac{1}{\xi g}\frac{\partial w^2}{\partial \zeta} + \frac{uw}{\xi g}\right]$$
$$= -\frac{1}{\xi g}\frac{\partial p}{\partial \zeta} - \frac{w}{(g\xi)^2} + \nabla^2 w + \frac{2}{(g\xi)^2}\frac{\partial u}{\partial \zeta} \tag{21}$$

$$PrRe\left[\frac{\partial T}{\partial t} + \frac{1}{\xi g}\frac{\partial \xi uT}{\partial \xi} - \frac{\xi g'}{g}\frac{\partial vT}{\partial \xi} + \frac{\partial vT}{\partial \eta} + \frac{1}{\xi g}\frac{\partial wT}{\partial \zeta}\right] = \nabla^2 T \tag{22}$$

$$\nabla^2 = \frac{1}{g^2}\left[\frac{1}{\xi} + \xi g'^2\right]\frac{\partial}{\partial \xi}\left(\xi\frac{\partial}{\partial \xi}\right) - \xi\frac{g''g - g'^2}{g^2}\frac{\partial}{\partial \xi} - \frac{2\xi g'}{g}\frac{\partial^2}{\partial \eta \partial \xi}$$
$$+ \frac{\partial^2}{\partial \eta^2} + \frac{1}{(\xi g)^2}\frac{\partial^2}{\partial \zeta^2} \tag{23}$$

The transformed boundary conditions become, at $\eta = 0$,

$$T = 0, \qquad u = 0, \qquad v = 0, \qquad w = 0 \tag{24}$$

and, at $\eta = 1$,

$$T = 1, \qquad u = 0, \qquad v = 0, \qquad w = 0 \tag{25}$$

At the interface ($\xi = 1$),

$$\left(\frac{1}{g} + \frac{g'^2}{g}\right)\frac{\partial T}{\partial \xi} - g'\frac{\partial T}{\partial \eta} = -NBiT \tag{26}$$

$$u = g'v \tag{27}$$

$$\left(\frac{1 + g'^2}{g}\right)\frac{\partial v}{\partial \xi} - 2g'\frac{\partial v}{\partial \eta} + \left(\frac{g' + g'^3}{g}\right)\frac{\partial u}{\partial \xi}$$
$$+ (1 - g'^2)\frac{\partial u}{\partial \eta} = -SN\frac{\partial T}{\partial \eta} \tag{28}$$

$$(1 + g'^2)\frac{\partial w}{\partial \xi} - gg'\left(\frac{\partial w}{\partial \eta} + \frac{1}{g}\frac{\partial v}{\partial \zeta}\right) - w + \frac{\partial u}{\partial \zeta} = -SN\frac{\partial T}{\partial \zeta} \tag{29}$$

The shape $[g(z)]$ of the interface with described liquid volume is determined by Eqs. (13) and (14). The transformed governing equations (18–22) and boundary conditions Eqs. (24–29) are solved by a finite volume method employing a SIMPLER algorithm. Nonuniform grids are constructed with finer meshes in the regions near the free surface and the upper and lower walls where boundary layers develop. To examine grid dependence, steady-state surface velocity and temperature distributions are computed with various grids and liquid volumes. Figures 2 and 3 show surface velocity and temperature grid-dependence with $Bi = 0$, $\mathit{AR} = 0.714$, $Pr = 27$, and $V = 1$ in two- and three-dimensional simulations as one example of grid-refinement studies. It is found that a steady-state is axisymmetric. Axisymmetric numerical results are in good agreement with those from three-dimensional simulations in a steady state. When the number of grid points increases, the peak of the unregularized velocity near the cold wall decreases and approaches to the regularized result as shown in Figs. 2 and 3. Stream function minima changed less than 5% regardless of regularization. Thus, a mesh of $51(r) \times 61(z)$ with regularization is used in our two-dimensional simulations. In the three-dimensional model, critical Reynolds numbers are computed with $Bi = 0$ and various grids and Prandtl numbers. Convergence criteria for a steady state are $|s^{n+1} - s^n| \le 10^{-10}$ and $|s^{n+1} - s^n|/|s^{n+1}| \le 10^{-4}$, where s is any variable, u, v, w, or T, at all points and n is time-marching level. Also, we checked time history of velocities and temperature at the midpoint of the

Table 1 Grid refinement studies of three-dimensional convection with $Bi = 0$

Grid numbers ($N_r \times N_z \times N_\theta$)	Re_c	Regularization
$\mathit{AR} = 1$, $V(R_r) = 1(1)$, $Pr = 1$		
$31 \times 31 \times 30$	2650	No
$41 \times 41 \times 40$	2580	No
$51 \times 51 \times 50$	2570	No
$31 \times 31 \times 30$	2550	Yes
$41 \times 41 \times 40$	2520	Yes
$51 \times 51 \times 50$	2520	Yes
$\mathit{AR} = 1$, $V(R_r) = 1(1)$, $Pr = 4$		
$31 \times 31 \times 30$	1060	Yes
$41 \times 41 \times 40$	1010	Yes
$51 \times 51 \times 50$	970	Yes
$\mathit{AR} = 0.714$, $V(R_r) = 1(0.714)$, $Pr = 27$		
$31 \times 41 \times 30$	220	Yes
$41 \times 51 \times 40$	210	Yes
$51 \times 61 \times 50$	220	Yes
$41 \times 51 \times 40$	200	No
$51 \times 61 \times 50$	200	No
$\mathit{AR} = 0.714$, $V(R_r) = 0.755(0.571)$, $Pr = 27$		
$41 \times 51 \times 40$	220	Yes
$51 \times 61 \times 50$	220	Yes

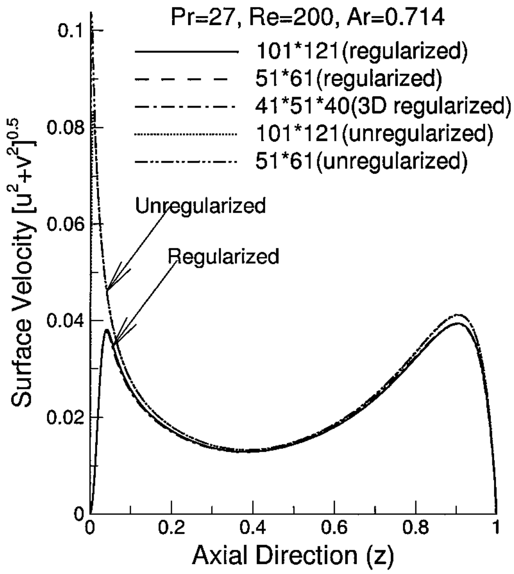

Velocity

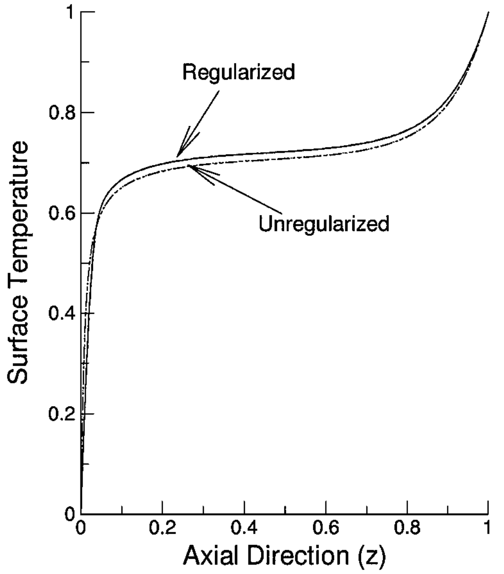

Temperature distributions

Fig. 2 Axisymmetric surface with various grids ($V=1$, $Pr=27$, and $Re=200$).

free surface. Table 1 shows Re_c found using different grids with $Bi=0$ and various Pr and V. The azimuthal direction has uniform grids, and Re is varied in increments of 10 to estimate Re_c. These steps, $\Delta Re=10$, in Re are less than 5% of the reported Re_c. The effect of regularization with $Pr=27$ and 1 on Re_c is about 5%, as shown in Table 1. Subsequent results are computed with a mesh of $41(r)\times 51(z)\times 40(\theta)$ for $V\leq 1$ and $51\times 61\times 50$ for $V=1.139$.

The axisymmetric code is validated by comparison of the minimum values of the stream functions with those from Sumner et al.[12] in Table 2. Table 3 shows Re_c, ω_c, and m from the three-dimensional simulations and linear theories.[17,19] The effect of regularization on Re_c, the stream function minima, and ω_c is less than 5%, as shown in Tables 1–3. Thus, the regularization is used to save computing time in all reported two- and three-dimensional simulations. The mesh of 51×61 with regularization is better than 101×121 without regularization in the aspect of saving computing time. In addition, the number of time iterations with regularization for steady state was about two times smaller than without regularization in three-dimensional simulations. More details on regularization may be found in Refs. 17 and 23.

Table 2 Comparison of stream function minima ($\psi_{\min}\times 10^2$) in a two-dimensional liquid bridge[a]

Re	Pr	Sumner et al.[12]	Present result without regularization	Present result with regularization
100	10	−0.4221	−0.4217	−0.4183
10	100	−0.4205	−0.4202	−0.4199

[a] $Bi=0.3$, $AR=1$, and $V=1$.

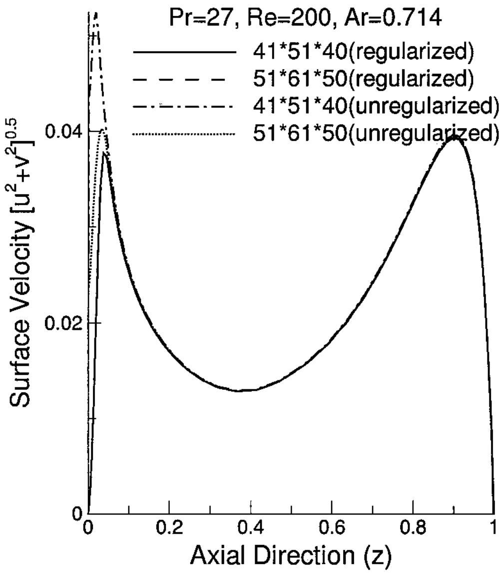

Velocity

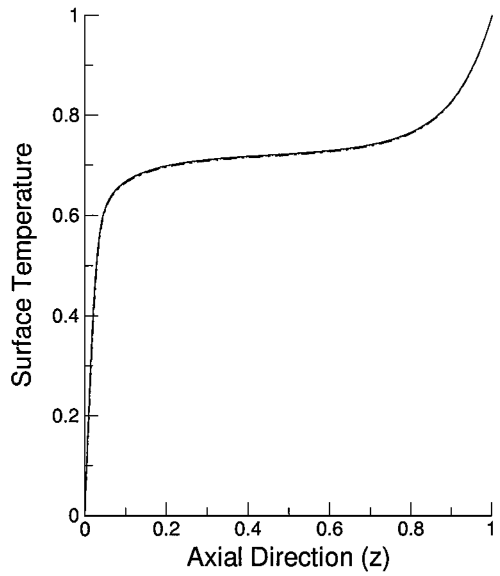

Temperature distributions

Fig. 3 Surface with various grids in three-dimensional simulations ($Bi=0$, $V=1$, $Pr=27$, and $Re=200$).

Results and Discussion

Axisymmetric Thermocapillary Convection with $Bi=0$, $AR=0.714$, $Pr=27$, and Various V

We have investigated thermocapillary convection with various V up to $Re=1000$ and have found no axisymmetric oscillatory states in a liquid bridge with either flat or curved surfaces. Thus, we conclude that only azimuthal waves can generate oscillations in this model, that is, time-dependent thermocapillary convection with $m=0$ does not occur in the liquid bridge. Whereas oscillatory thermocapillary convection in a rectangular cavity can be investigated in two-dimensional simulations,[30] it cannot be realized in an

Table 3 Comparison with linear stability analysis for $Pr = 1$ and 4[a]

	Present results (regularization)			Present results (no regularization)			Linear stability[17] (regularization)			Linear stability[19] (no regularization)		
Pr	Re_c	ω_c	m	Re_c	ω_c	m	Re_c	ω_c	m	Re_c	ω_c	m
1	2520	58.0	2	2580	58.7	2	2539	63.2	2	2551	65.0	2
4	1010	25.1	2	——	——	——	1047	27.9	2	1002	28.5	2

[a] $Bi = 0$, $AR = 1$, and $V = 1$.

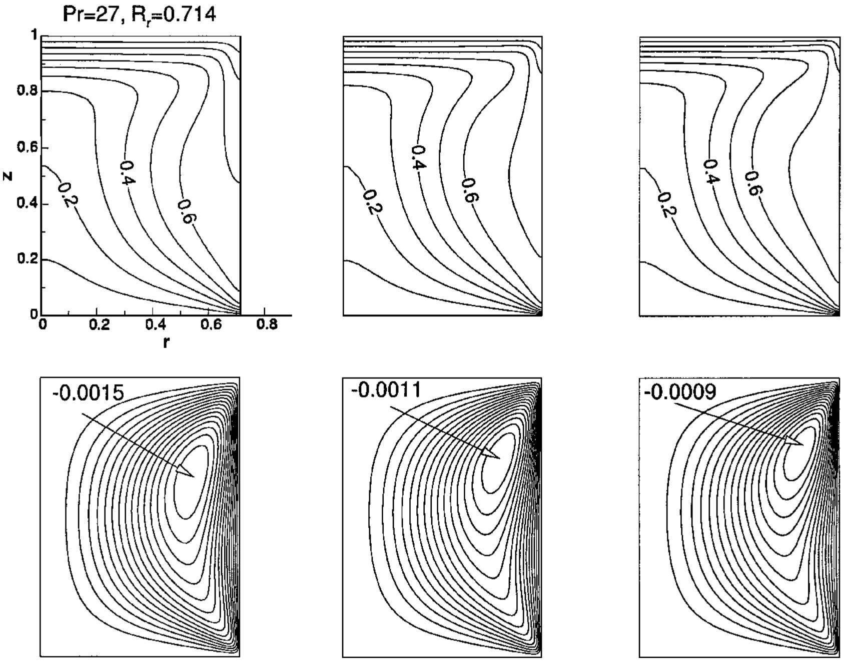

a) b) c)

Fig. 4 Axisymmetric isotherms and streamlines with $Bi = 0$, $AR = 0.714$, $V = 1$, $Pr = 27$ and a) $Re = 100$, b) $Re = 200$, and c) $Re = 300$.

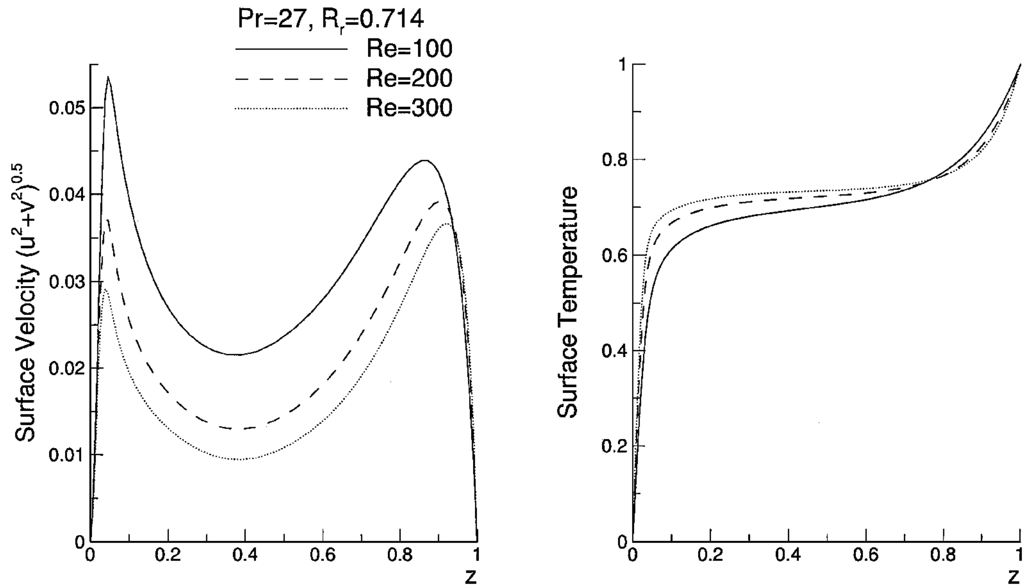

a) b)

Fig. 5 Surface a) velocity and b) temperature corresponding to Fig. 4.

open cylinder ($AR = 1$ and $Pr = 30$) with a uniform heat flux[27] or in a liquid bridge ($AR = 0.714$ and $Pr = 30$). Oscillatory buoyant-thermocapillary convection was reported in axisymmetric simulations by Shevtsova and Legros,[23] but no oscillations of pure thermocapillary convection were found in their axisymmetric simulations.

Figure 4 shows isotherms and streamlines with a cylindrical surface and various Reynolds numbers. The corresponding surface velocity and temperature distributions are shown in Fig. 5. The maximum dimensionless velocity and stream function decrease with increasing Reynolds number as expected.[28] The center of recirculation cells moves closer to the hot wall with increasing Reynolds number. Only a single cell is available in two-dimensional studies. The flows with curved surfaces are shown in Figs. 6 and 7 to have patterns similar to that with a flat surface. The flowfields with various V show a large toroidal flow (without a secondary vortex), which is a characteristic of steady thermocapillary convection.

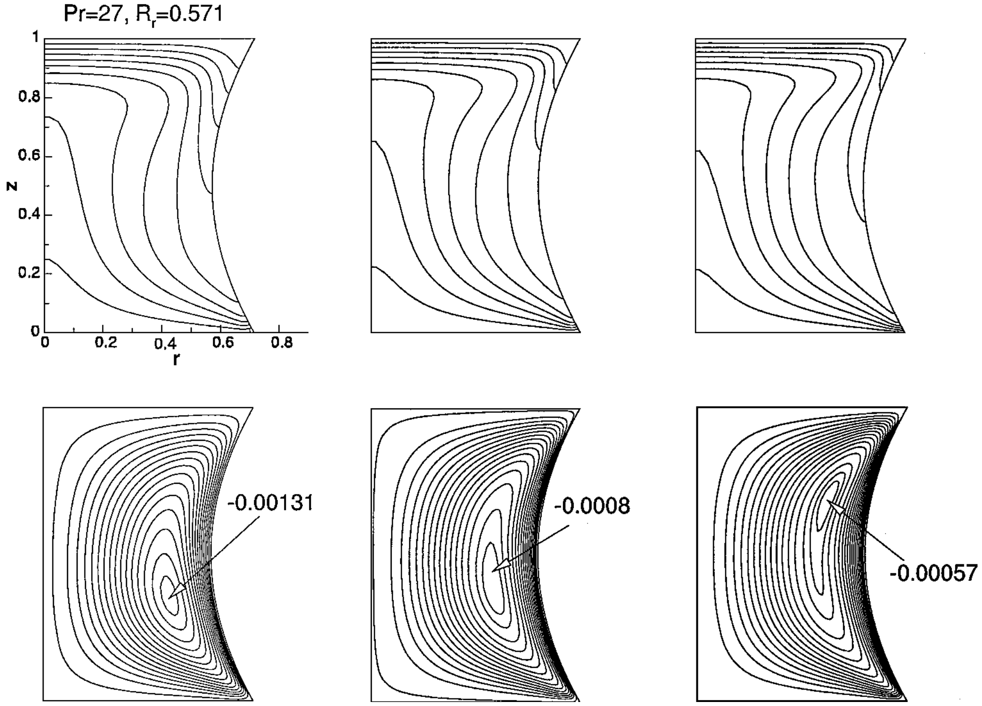

a) b) c)

Fig. 6 Axisymmetric isotherms and streamlines with $Bi = 0$, $AR = 0.714$, $V = 0.755$, $Pr = 27$ and a) $Re = 100$, b) $Re = 200$, and c) $Re = 300$.

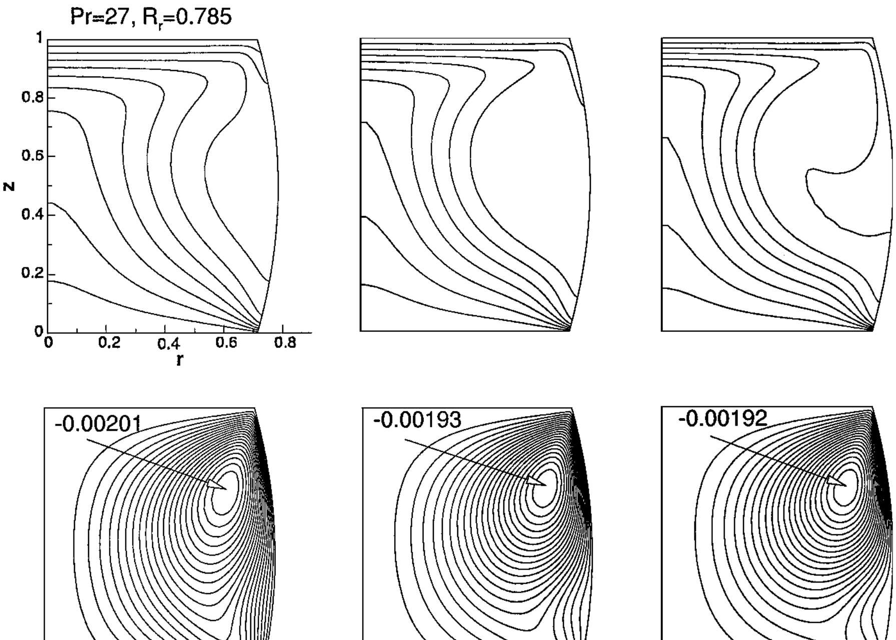

a) b) c)

Fig. 7 Axisymmetric isotherms and streamlines with $Bi = 0$, $AR = 0.714$, $V = 1.138$, $Pr = 27$ and a) $Re = 100$, b) $Re = 200$, and c) $Re = 300$.

A secondary vortex can appear in steady buoyant-thermocapillary convection.[12,23]

Three-Dimensional Thermocapillary Convection with $Bi = 0$, $AR = 0.714$, and $Pr = 27$

The critical Reynolds number Re_c for onset of oscillations with a flat cylindrical surface is about 210. At this critical Reynolds number, the flow is steady, and the isotherms on the free surface are just circular lines, that is, axisymmetric. Figure 8 shows the time history of the temperature near the midpoint of the free surface at three supercritical Reynolds number values. Figures 8a–8c are computed from the same steady-state initial conditions, $Re = 200$. Oscillations begin earlier in time at higher Reynolds number. Figures 9a and 9b show temperature fluctuations in the section $z = 0.53$ and at the free surface for $Re = 230$ with $V = 1$ and 1.138 ($Re_c = 210$), respectively. Figure 10 shows temperature signals from four numerical thermocouples at different azimuthal positions. The temperature fluctuations consist of a hot and a cold spot rotating clockwise, that is, $m = 1$. This rotating pattern with $m = 1$ remained unchanged with increasing Reynolds number beyond the critical value.

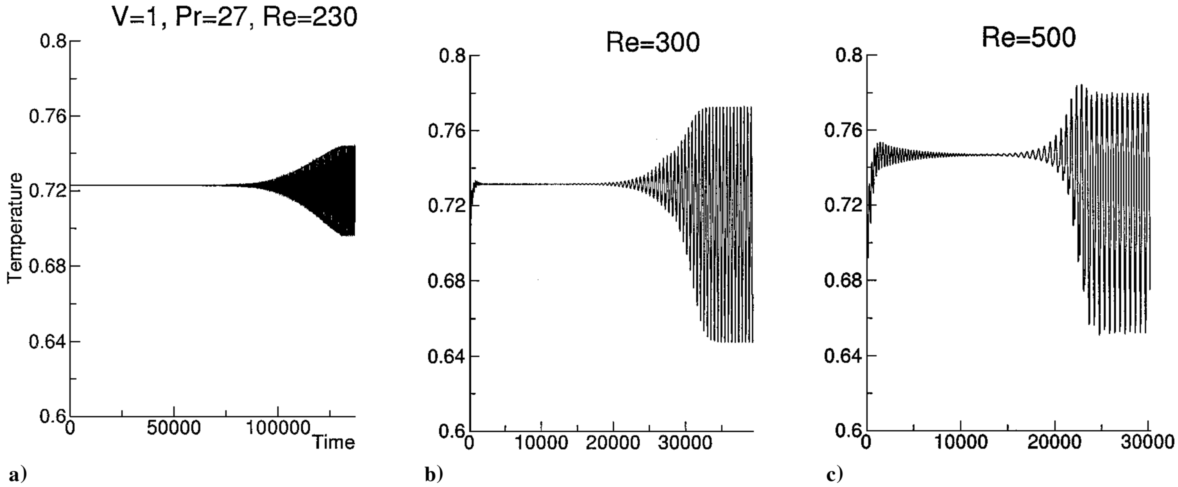

Fig. 8 Time history of the temperature near the midpoint of the free surface with *Bi* = 0, *A*R = 0.714, *V* = 1, and *Pr* = 27.

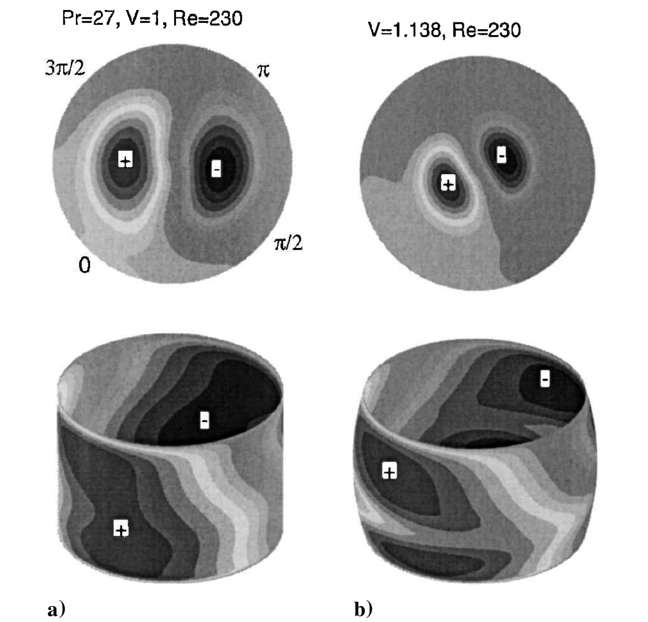

Fig. 9 Snapshots of temperature fluctuations in the section (*z* = 0.53) and the free surface with *Bi* = 0, *A*R = 0.714, and various *V*.

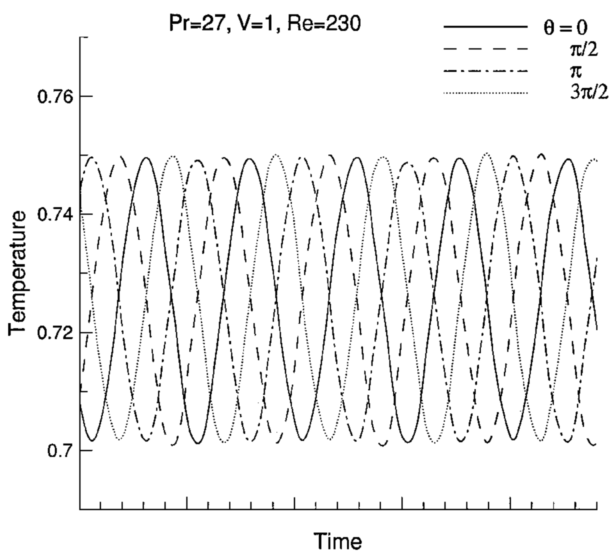

Fig. 10 Temperature oscillations at four fixed points with *r* = 1, *z* = 0.53, *θ* = 0, *π*/2, *π*, and 3*π*/2, corresponding to Fig. 9a.

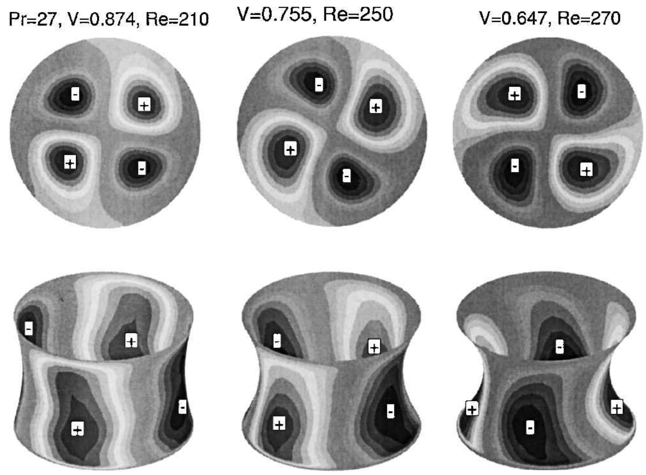

Fig. 11 Snapshots of temperature fluctuations in the section *z* = 0.53 and the free surface with *Bi* = 0, *A*R = 0.714, and various *V*.

Re_c was found to decrease with increasing V in the case of concave surfaces. With $V = 0.874$, 0.755, and 0.647, Re_c are found to be about 190, 220, and 250, respectively. Figure 11 shows temperature fluctuations in the section $z = 0.53$ and at the free surface with various V. Two pairs of hot and cold spots, that is, a wave number of 2, are rotating clockwise.

Critical Reynolds Number and Wave Number

Figure 12 shows the variation of Re_c and m with V. Heat loss from the free surface stabilizes the flow as it tends to decrease the free surface temperature gradient, and Re_c increases with increasing Bi. With $Bi = 0$, two kinds of wave numbers are observed, and a transition from $m = 1$ to 2 occurs at V of about 0.9. The wave number can change with Bi. This change in wave number was reported in experiments,[11] where a wave number of 1 was changed into 2 by altering the surrounding conditions of a liquid bridge.

Heat loss to surroundings is through forced convection induced by the action of shear stresses at the free surface. The value of h for gases in forced convection is in the range 25–250 W/(m^2 K). With $H = 1.4$ mm in experiments,[10] Bi is in the range 0.32–3.2. In the three-dimensional numerical simulations with a cylindrical surface and $Pr = 7$ of Ref. 24, $Bi = 6.4$ was necessary to compare with the experimental results of Ref. 2. Thus, our $Bi = 1$ (a much smaller bridge) is a reasonable assumption to compare with the experimental results of Ref. 10. In addition, previous work[31–33] showed that the inclusion of surface heat loss was necessary to achieve better agreement with experiments. When our numerical results with $Bi = 1$ are compared with those from normal gravity experiments,[10]

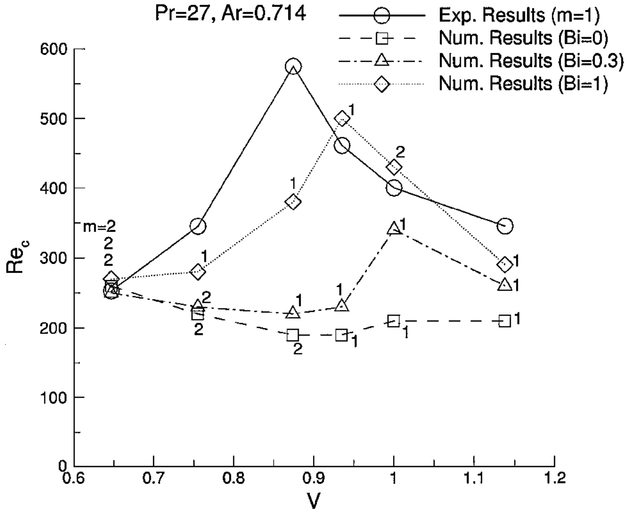

Fig. 12 Variations of Reynolds number Re_c and m with Biot number with experimental results from Ref. 10; two different branches are observed in the stability diagram with $Bi > 0$.

the wave number of 1 and the rotating mode are in good agreement. With $V = 1$, transition to $m = 1$ from $m = 2$ occurs at $Bi = 0.5$. Re_c is about 400 and wave number is 1 with $V = 1$ and $Bi = 0.5$. With $Bi > 0$, it is found that two different branches can exist in the stability diagram ($V - Re_c$). The most stable range of V with $Bi = 1$ is near 0.94, which is not in good agreement with experimental result,[10] $V = 0.87$ (Ref. 10). However, in experiments by Sumner et al.[12] at a higher Prandtl number Pr, the most stable range was near $V = 0.95$. Other experiments[11] showed that range was very close to $V = 1$. Although the experiments were performed with small rods, the difference between numerical and experimental results may be due to gravity-induced bridge deformation because the largest static Bond number ($Bd = \rho g H^2/\sigma$) was 2 in the experiments.[10]

Conclusions

Two- and three-dimensional thermocapillary convection in a cylindrical liquid bridge is investigated numerically to document its stability characteristics. Two-dimensional simulations with cylindrical or curved free surfaces predict steady convection even at very high Reynolds numbers. It is found that only azimuthal waves can generate oscillations in the model. The stream function minima and the maximum surface velocity and temperature decrease with increasing Reynolds number.

Oscillatory thermocapillary convection is possible only in three-dimensional calculations. This is consistent with experiments. With $Bi = 0$ and either a flat or a convex surface, waves with the wave number of 1 are rotating clockwise. The pattern remains unchanged with increasing Reynolds number beyond the critical value. The wave number of 2 is observed with $Bi = 0$ and a concave surface, and the waves are also rotating clockwise. Heat loss from the free surface stabilizes the flow, and critical Reynolds number increases with increasing Biot number. The wave number changes with Biot number. With $Bi > 0$, it is found that two different branches can exist in the stability diagram ($V - Re_c$). The results with $Bi = 1$ are in reasonable agreement with available normal gravity experiments although these seem to favor a single azimuthal wave.

Acknowledgment

We gratefully acknowledge computer resources from the Rutgers Computational Grid composed of a Distributed Linux personal computer cluster on which all computations were performed.

References

[1]Schwabe, D., "Marangoni Effects in Crystal Growth Melts," *PhysicoChemical Hydrodynamics*, Vol. 2, No. 4, 1981, pp. 263–280.

[2]Preisser, F., Schwabe, D., and Scharmann, A., "Steady and Oscillatory Thermocapillary Convection in Liquid Columns with Free Cylindrical Surface," *Journal of Fluid Mechanics*, Vol. 126, 1983, pp. 545–567.

[3]Velten, R., Schwabe, D., and Scharmann, A., "The Periodic Instability of Thermocapillary Convection in Cylindrical Liquid Bridges," *Physics of Fluids*, Vol. 3, No. 2, 1991, pp. 267–279.

[4]Carotenuto, L., Castagnolo, D., Albanese, C., and Monti, R., "Instability of Thermocapillary Convection in Liquid Bridges," *Physics of Fluids*, Vol. 10, No. 3, 1998, pp. 555–565.

[5]Monti, R., Savino, R., and Lappa, M., "Flight Results on Marangoni Flow Instability in Liquid Bridges," *Acta Astonautica*, Vol. 47, Nos. 2–9, 2000, pp. 325–334.

[6]Muehlner, K., Schatz, M., Petrov, V., McCormick, W., Swift, J., and Swinney, H., "Observation of Helical Traveling-Wave Convection in a Liquid Bridge," *Physics of Fluids*, Vol. 9, No. 6, 1997, pp. 1850–1852.

[7]Schwabe, D., and Frank, S., "Experiments on the Transition to Chaotic Thermocapillary Flow in Floating Zones Under Microgravity," *Advances in Space Research*, Vol. 24, No. 10, 1999, pp. 1391–1396.

[8]Schwabe, D., and Velten, R., "The Multi-Roll-Structure of Thermocapillary Flow and Its Transition to Oscillatory Flow in Long Floating Zones with Length L near the Rayleigh-Limit and Restationarization Above the Critical Marangoni Number," *Journal of the Japan Society of Microgravity Applications*, Vol. 15, Supplement 2, 1998, pp. 425–430.

[9]Hu, W., Shu, J., Zhou, R., and Tang, Z., "Influence of Liquid Bridge Volume on the Onset of Oscillation in Floating Zone Convection. I. Experiments," *Journal of Crystal Growth*, Vol. 142, Nos. 3–4, 1994, pp. 379–384.

[10]Masud, J., Kamotani, Y., and Ostrach, S., "Oscillatory Thermocapillary Flow in Cylindrical Columns of High Prandtl Number Fluids," *Journal of Thermophysics and Heat Transfer*, Vol. 11, No. 1, 1997, pp. 105–111.

[11]Shevtsova, V., Mojahed, M., and Legros, J., "The Loss of Stability in Ground Based Experiments in Liquid Bridges," *Acta Astronautica*, Vol. 44, Nos. 7–12, 1999, pp. 625–634.

[12]Sumner, L., Neitzel, G., Fontaine, J.-P., and Dell'Aversana, P., "Oscillatory Thermocapillary Convection in Liquid Bridges with Highly Deformed Free Surfaces: Experiments and Energy-Stability Analysis," *Physics of Fluids*, Vol. 13, No. 1, 2001, pp. 107–120.

[13]Smith, M., and Davis, S., "Instabilities of Dynamic Thermocapillary Liquid Layers: Part 1. Convective Instabilities," *Journal of Fluid Mechanics*, Vol. 132, 1983, pp. 119–144.

[14]Xu, J.-J., and Davis, S., "Convective Thermocapillary Instabilities in Liquid Bridges," *Physics of Fluids*, Vol. 27, No. 5, 1984, pp. 1102–1107.

[15]Kuhlmann, H., and Rath, H., "Hydrodynamic Instabilities in Cylindrical Thermocapillary Liquid Bridges," *Journal of Fluid Mechanics*, Vol. 247, 1993, pp. 247–274.

[16]Levenstam, M., and Amberg, G., "Hydrodynamic Instabilities of Thermocapillary Flow in a Half-Zone," *Journal of Fluid Mechanics*, Vol. 297, 1995, pp. 357–372.

[17]Wanschura, M., Shevtsova, V., Kuhlmann, H., and Rath, H., "Convective Instability Mechanisms in Thermocapillary Liquid Bridges," *Physics of Fluids*, Vol. 7, No. 5, 1995, pp. 912–925.

[18]Neitzel, G., Chang, K.-T., Jankowski, D., and Mittelmann, H., "Linear-Stability Theory of Thermocapillary Convection in a Model of the Float-Zone Crystal-Growth Process," *Physics of Fluids*, Vol. 5, No. 1, 1993, pp. 108–114.

[19]Levenstam, M., Amberg, G., and Winkler, C., "Instabilities of Thermocapillary Convection in a Half-Zone at Intermediate Prandtl Numbers," *Physics of Fluids*, Vol. 13, No. 4, 2001, pp. 807–816.

[20]Chen, Q., and Hu, W., "Influence of Liquid Bridge Volume on Instability of Floating Half Zone Convection," *International Journal of Heat and Mass Transfer*, Vol. 41, Nos. 6–7, 1998, pp. 825–837.

[21]Tao, Y., Sakidja, R., and Kou, S., "Computer Simulation and Flow Visualization of Thermocapillary Flow in a Silicone Oil Floating Zone," *International Journal of Heat and Mass Transfer*, Vol. 38, No. 3, 1995, pp. 503–510.

[22]Savino, R., and Monti, R., "Oscillatory Marangoni Convection in Cylindrical Liquid Bridges," *Physics of Fluids*, Vol. 8, No. 11, 1996, pp. 2906–2922.

[23]Shevtsova, V., and Legros, J., "Oscillatory Convective Motion in Deformed Liquid Bridges," *Physics of Fluids*, Vol. 10, No. 7, 1998, pp. 1621–1634.

[24]Leypoldt, J., Kuhlmann, H., and Rath, H., "Three-Dimensional Numerical Simulation of Thermocapillary Flows in Cylindrical Liquid Bridges," *Journal of Fluid Mechanics*, Vol. 414, 2000, pp. 285–314.

[25]Shevtsova, V., Melnikov, D., and Legros, J., "Three-Dimensional Simulations of Hydrodynamic Instability in Liquid Bridges: Influence of Temperature-Dependent Viscosity," *Physics of Fluids*, Vol. 13, No. 10, 2001, pp. 2851–2865.

[26]Lappa, M., Savino, R., and Monti, R., "Three-Dimensional Numerical Simulation of Marangoni Instabilities in Non-Cylindrical Liquid Bridges in

Microgravity," *International Journal of Heat and Mass Transfer*, Vol. 44, No. 10, 2001, pp. 1983–2003.

[27]Sim, B.-C., and Zebib, A., "Thermocapillary Convection in Open Cylinders with Undeformable Curved Surfaces," *International Journal of Heat and Mass Transfer* (to be published).

[28]Zebib, A., Homsy, G., and Meiburg, E., "High Marangoni Number Convection in a Square Cavity," *Physics of Fluids*, Vol. 28, No. 12, 1985, pp. 3467–3476.

[29]Mundrane, M., and Zebib, A., "Low Prandtl Number Marangoni Convection with a Deformable Interface," *Journal of Thermophysics and Heat Transfer*, Vol. 9, No. 4, 1995, pp. 795–797.

[30]Xu, J., and Zebib, A., "Oscillatory Two- and Three-Dimensional Thermocapillary Convection," *Journal of Fluid Mechanics*, Vol. 364, 1998, pp. 187–209.

[31]Sim, B.-C., and Zebib, A., "Effect of Surface Heat Loss and Rotating on Transition to Oscillatory Thermocapillary Convection," *Physics of Fluids*, Vol. 14, No. 1, 2002, pp. 225–231.

[32]Schwabe, D., Zebib, A., and Sim, B.-C., "Oscillatory Thermocapillary Convection in Open Cylindrical Annuli. Part 1. Experiments Under Microgravity," *Journal of Fluid Mechanics* (submitted for publication).

[33]Sim, B.-C., Zebib, A., and Schwabe, D., "Oscillatory Thermocapillary Convection in Open Cylindrical Annuli. Part 2. Simulations," *Journal of Fluid Mechanics* (submitted for publication).